MR of Slow CSF Flow in the Spine

Dieter Schellinger, Denis LeBihan, Sunder S. Rajan, Curtis A. Cammarata, Nicholas J. Patronas, John P. Deveikis, and Lucien M. Levy

PURPOSE: To evaluate a slow-flow MR sequence in normal CSF flow and in CSF flow disturbance in cases of spinal stenosis. **METHOD:** The method was tested for flow sensitivity and applied to 67 sites of spinal canal compromise. **RESULTS:** Phantom studies show that flow can be depicted at a velocity of 0.5–1 mm/sec. On clinical images, stagnant CSF is black, flowing CSF is bright. Typically, in high-grade (90%–100%) stenosis, CSF above and below the site of spinal canal compromise (SCC) is black. With intermediate stenosis (50%–89%), CSF above the SCC remains white but becomes black distal to the SCC. Low-grade stenosis shows only localized flow disturbances. **CONCLUSION:** This easy-to-use sequence can solidify the MR diagnosis of high-grade stenosis when a distinct flow pattern is recognized. Flow patterns for intermediate and low-grade stenosis are less reliable.

Index terms: Spine, stenosis; Spinal cord, magnetic resonance; Cerebrospinal fluid, flow dynamics

AJNR 13:1393–1403, Sep/Oct 1992

While intracranial (1–12) and spinal (13–21) CSF flow have been evaluated with a variety of imaging schemes, the methods are either not sensitive to slow flow or lack speed and ease of application. This paper has a dual purpose: It introduces and appraises an optimized slow flow magnetic resonance (SFMR) sequence and describes flow changes as observed with variable degrees of spinal stenosis.

The sequence has a high sensitivity to slow flow, can be implemented with ease, requires little scanning time, and may be used as an addendum to any routine imaging protocol. The design is based on an optimized 3-D steady-state free precession (SSFP) scheme (22). SSFP has been previously applied by Jolesz and Patz (7, 8). However, these authors used a different scheme and applied the sequence only to brain-related pathologies and conditions.

In this paper, SFMR is applied to cerebrospinal fluid (CSF) flow along the spinal axis. The flow changes of spinal canal stenosis are investigated. It is expected that various degrees of spinal stenosis will show different flow patterns. CSF velocity images may improve the diagnostic process by adding physiologic information to existing anatomic data.

Received July 8, 1991; accepted and revision requested September 4; revision received December 3 and accepted December 8.

All authors: Department of Radiology, Division of Neuroradiology, Georgetown University Medical Center, 3800 Reservoir Rd, NW, Washington, DC 20007. Address reprint requests to Dieter Schellinger, MD.

AJNR 13:1393–1403, Sep/Oct 1992 0195-6108/92/1305-1393

Materials and Methods

Sequence Design and Image Processing

The sequence diagram is shown in Figure 1. It is based on a gradient-echo, low flip angle scheme. This type of sequence has a built-in sensitivity to slow flow, as suggested by Patz (7). Special features have been added to increase sensitivity to slow flow. For example, the configuration of the gradient pulses on the readout axis was designed in such a way that the signal preceding each RF pulse is monitored while the signal following each pulse is destroyed by the first gradient pulse, as suggested by Hawkes and Gyngell (CE-FAST) (23, 24). Also, a symmetric disposition of the gradient pulses on the section-selective and phase-encoding axes was aimed at enforcing transverse magnetization coherence for static spins (SSFP) (23). This design renders the scheme highly sensitive to any dephasing produced by in-lane flowing spins, mainly in the direction of the readout gradient and results in a refocusing defect on the echo. It produces a dramatic loss of signal and an enhanced flow-void effect and leads to greater sensitivity for slow-flow imaging. As it stands, the sequence does not provide directional and absolute quantitative velocity data. Maximum flow sensitivity is obtained along the readout direction. The sequence was implemented in a 3-

D acquisition mode. There was no use of presaturation anterior to the imaging volume.

A 1.5-T MR whole body scanner was used. Image parameters included a TE of 6 msec, sampling time of 3 msec, TR of 16 msec, a flip angle of 30°, a 256 × 256 matrix, and a single excitation. The 3-D slab thickness was 40 mm, with 16 or 32 partitions resulting in a total imaging time of 1 min 9 sec or 2 min 18 sec, respectively. The sequence does not require cardiac triggering and there are no special gradient requirements. Commercial unshielded gradient coils were used (10 mT/m). Since there are no particular hardware needs, the sequence can be adapted to any MR scanner which supports this type of scheme. Thus, programming of the sequence for its use on other scanners should be straightforward. Since there is only a minimal time penalty to be paid, this slow-flow scheme was routinely added to all spine MR scans.

In this study, only the 2-D raw images of the 3-D set were used. Projections with a tilted new angle can be obtained using a ray-tracer projection algorithm. This would be conceptionally beneficial for obtaining angiograms with this sequence, but was not used here. The 3-D mode was chosen mainly to increase the signal-to-noise level.

Critical to the success of the method is achievement of a good contrast between the flow void and the signal of the static structures. The acquisition parameter combination (flip angle, TR, TE) mentioned above was optimized to maximize the flow signal against the static background

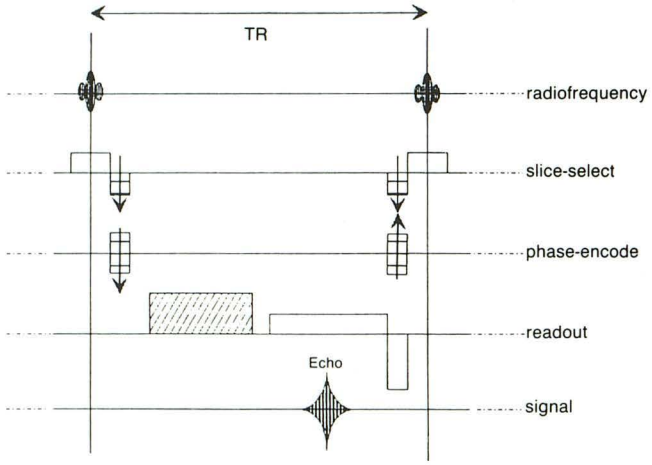

Fig. 1. Sequence diagram. Symmetric and balanced gradients about the echo for the section select and the phase-encoding assures phase coherence between RF pulses for stationary tissues, a necessary condition for the establishment of SSFP. This arrangement produces two signal formations, one following each RF pulse (echo 1), the other preceding each RF pulse (echo 2). The readout gradient is designed such that only echo 2 is monitored, resulting in the well known CE-FAST type sequence. The dashed gradient on the readout axis is responsible for the slow-flow sensitivity of the sequence in the readout direction. It randomly spoils the transverse magnetization of flowing spins from one RF pulse to the next, preventing the build up of transverse coherence. Furthermore, this gradient pulse removes parts of susceptibility artifacts by adding a resonant offset that is averaged over 2-D across each pixel, whatever is its location in the image.

tissues. In images thus obtained, static tissues appear in bright gray tones, while flowing structures are black. Since this SFMR sequence was originally developed for imaging of slow vascular flow, the gray scale was reversed to help achieve the traditional angiographic presentation: flowing blood is white and static background tissues are dark. In the reversed gray scale mode used here for clinical imaging, higher velocity CSF flow is bright and static CSF is black. Furthermore, this display mode may facilitate recognition of details in flowing structures since it appears easier to detect bright details on a dark background.

All cases had sagittal and parasagittal SFMR images and the flow observations are based on these planes only. The frequency-encoding (readout) gradient was placed along the Z-axis. This sensitizes the images to flow in the longitudinal direction of the spinal canal.

Phantom Work

To calculate the sensitivity of the sequence to flow, a suitable phantom was built. The flow phantom was composed of a stretch of polyethylene tubing (3 mm inner diameter), with a constriction in the center. The channels are embedded in gel matrix. A 100-mL plastic bottle containing a sample of the flow medium (aqueous copper sulfate) was placed next to the flow system for intensity comparisons (Fig. 2). A continuous variable, nonpulsatile flow was achieved by siphoning the flowing medium from a reservoir that was placed on the table. The flow velocity was adjusted by changing the height of the receptacle to that of the reservoir. The phantom was placed inside a head imaging coil with the flow direction parallel to the Z axis. Flow rates from 0 to 60 mm/sec were determined by using a measuring cylinder and a stop watch.

Clinical Material

The sequence was used in well over 4000 head and spine cases. For spine studies, a circular polarized body coil was used for excitation and a surface coil was used for signal detection. In this material, there were 60 patients with various degrees of spinal canal stenosis or blockage in 67 anatomic areas (lumbar = 15, thoracic = 21, cervical = 31). The causative pathologies are detailed in Table 1. The degree of stenosis was appraised by reviewing sagittal and axial MR images and were estimated as severe (90%–100%), moderate (50%–89%) or mild (<49%) (Table 2). The corresponding CSF flow pattern was then analyzed. Twenty-three areas had myelographic correlation. The myelograms were performed in a temporal distance of up to 1 week and taken before initiation of therapy. In this paper, no attempt was made to analyze the diagnostic acumen of SFMR versus myelography. A larger number of cases would be needed to make such a comparison approximate the degree of stenosis and for comparing MR flow patterns with myelographic findings.

Results

Phantom Studies

The phantom work demonstrates how the signal drops in the presence of slow flow. The results are shown in Table 3. The sequence demonstrated very high sensitivity to slow flow. This is documented in Figure 2 with the corresponding intensity profile across the flowing and stationary sample for a flow velocity of 0, 1, and 4.5 mm/sec, respectively. Stationary fluid shows maximum brightness (100%). At a velocity of 1 mm/sec, the signal intensity is reduced to 56%. Thus, flow can be recognized at a velocity level of approximately 0.5–1 mm/sec. At 4.5 mm/sec, the signal intensity is almost totally decayed (9%). Velocities in the range of 0.5–4.5 mm/sec can be found in smaller veins, terminal arteries, and in CSF. The flow sensitivity was much larger when the direction of the flow was parallel to the frequency-encode axis, while the flow sensitivity was not as good for the phase-encode directions, as expected from the sequence design.

TABLE 3: Signal ratio (flowing/stationary) vs flow velocity

Velocity (mm/sec)	Ratio (flowing/stationary)
0	1.00
1	0.56
3	0.20
4.5	0.09
6	0
18	0
60	0

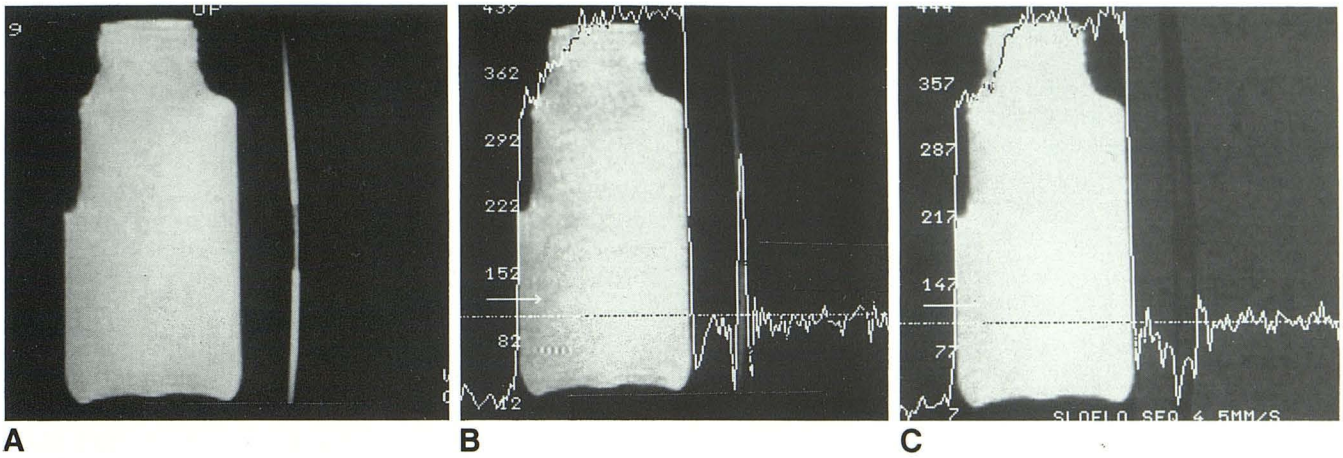

Fig. 2. Phantom studies. Signal drop in the presence of slow flow is shown. The phantom was made of a tube (3-mm inner diameter) with a constriction in the middle. A 100-mL plastic bottle filled with the flow medium (copper sulfate-doped water) was placed next to the tube for signal intensity comparisons.

A, No flow. Both the tube and the bottle display the same intensity.

B, Very slow flow (v = 1 mm/sec). The signal intensity in the tube has significantly decreased (56% attenuation).

C, At a flow rate of v = 4.5 mm/sec, the signal intensity is almost totally decayed (9%).

TABLE 1: Spinal canal compromise

HNP/focal degeneration	13[a] (6)[b]
Multilevel degeneration	16 (5)
Trauma	10 (2)
Metastases	15 (6)
Congenital	4 (3)
Tumors (cord, intradural)	9 (1)
Total	67 (23)

Note. — HNP, herniated nucleus pulposus.

[a] No. of areas examined.

[b] No. of areas examined with myelography.

TABLE 2: Degree of spinal canal compromise

90%–100%	28[a] (10)[b]
50%–89%	13 (6)
10%–49%	12 (7)
Total	67 (23)

[a] No. of areas examined.

[b] No. of areas examined with myelography.

Normal Signal Patterns

In our phantom work, it was demonstrated that there is dramatic signal drop off in the presence of slow flow. Stagnant CSF was white and flowing CSF became progressively dephased and was rendered in black. For clinical imaging, it was deemed more practical to reverse the contrast, so that flowing structures would appear brighter

than static structures. Thus, image appearance would match with that of traditional angiograms.

In all cases, CSF of the normal cervical and thoracic canal imaged in white, contrasting with the normal spinal cord that is portrayed in dark gray or black (Fig. 3A). The bright signals emanating from CSF reflect a velocity range of 5 mm/sec and over. Since this sequence is T2*-weighted and images are viewed in the black-white reversed mode, all stationary tissues that are traditionally shown in white will appear black and vice versa. Therefore, epidural fat is shown in black and the spinal column in white. Flowing substances will be imaged corresponding to their velocity range (Fig. 2).

In the upper lumbar region, CSF continues to image brightly. In the lower lumbar area, approximately at L5, the CSF flow pattern can be quite variable and shows a signal spectrum bridging from bright to black (Fig. 3B).

Abnormal Signal Patterns

Several CSF velocity patterns were observed. These could be assigned to three major groups of spinal canal compromise.

1. High Grade Stenosis (90%–100%) (type 1 pattern; Fig. 4; Table 4). A most distinctive flow pattern (type 1 pattern) was seen in 21 stenosed areas, eight of which were also examined with myelograms. All stenoses were in the thoracic

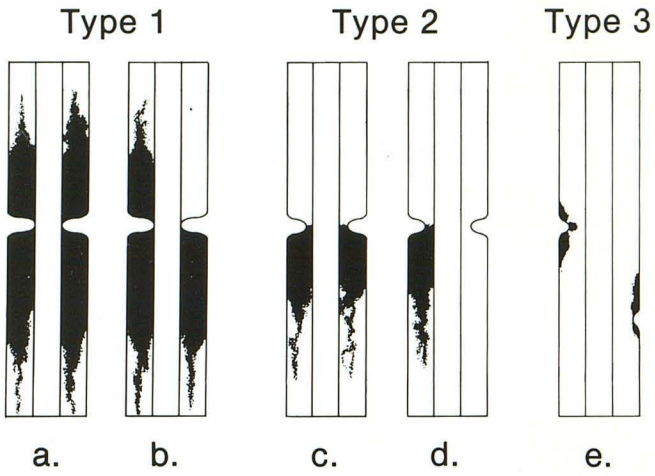

Fig. 4. Schematic drawings of velocity patterns with various degrees of spinal canal compromise (SCC). Cord (central band) divides CSF space into two compartments.

a, Type 1 pattern with attenuated CSF above and below level of SCC.

b, Type 1 pattern variant. CSF is attenuated both above and below level of SCC. One CSF compartment, above level of SCC, maintains higher velocity CSF.

c and *d*, Type 2 patterns. These velocity patterns were seen with intermediate grade stenosis.

e, Type 3 patterns. Focal velocity changes.

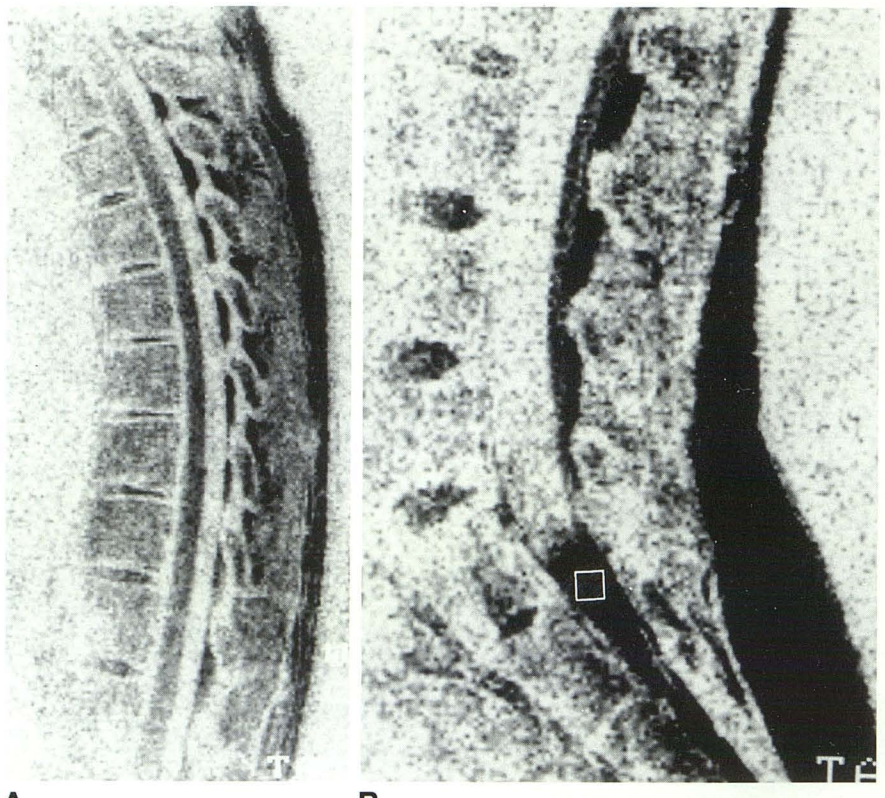

Fig. 3. Normal CSF flow in thoracic and lumbar spinal canal. In these and all other clinical images, the gray scale has been reversed when compared to the phantom work. No flow is rendered in black and flow is shown in various gray tones or in white.

A, Thoracic canal with cord and surrounding CSF. Portrayal of CSF in white indicates that the velocity is at or above threshold level (4.5 mm/sec).

B, The CSF velocity in the lumbar canal becomes attenuated as it reaches the distal end. White CSF becomes gray and then, black. Distal black fluid column represents stationary CSF (*white square*).

TABLE 4: Flow changes with spinal canal compromise

Percent of Stenosis	No. Areas Examined	No. Areas with Abnormal Flow	CSF Appearance Above/Below SSC
90–100	28 (10)	28 (10)	Type 1 pattern: 21 (8) black/black Pattern variant: 7 (2) black in anterior or posterior compartment/ black
50–89	13 (6)	9 (2)	Type 2 pattern: 3 (1) white/black Pattern variant: 6 (1) white/black in anterior or posterior compartment
10–49	26 (7)	11 (2)	Type 3 pattern: 11 (2) focal CSF blackening in area of stenosis

Note.—Numbers in parentheses indicate number of areas examined with myelography. SSC, spinal canal compromise.

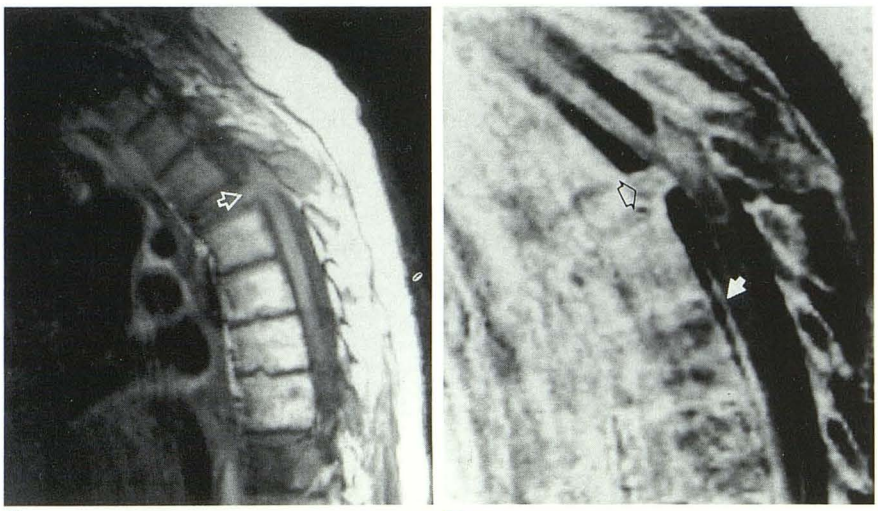

Fig. 5. Type 1 pattern. Total block in midthoracic region (*open arrows*) secondary to retrovertebral extension of metastatic process.

A, T1W spin-echo image.

B, Corresponding slow-flow image. CSF column above and below SCC is black. Distal to block and anterior to cord (*white arrow*), CSF regains velocity and becomes white.

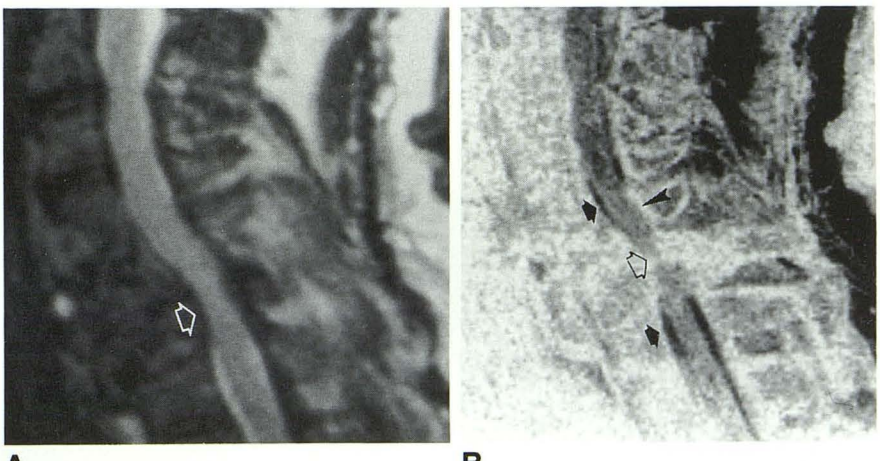

Fig. 6. Type 1 pattern. Total block in lower cervical areas (*open arrow*) due to compression of C6.

A, Sagittal T2*-weighted gradient-echo image of cervical spine shows focal effacement of CSF spaces.

B, Corresponding slow-flow image shows CSF above and below block in black (*black arrows*). Note: the white linear structure above the block (*arrowhead*) denotes cortical bone of spinous process, and not CSF.

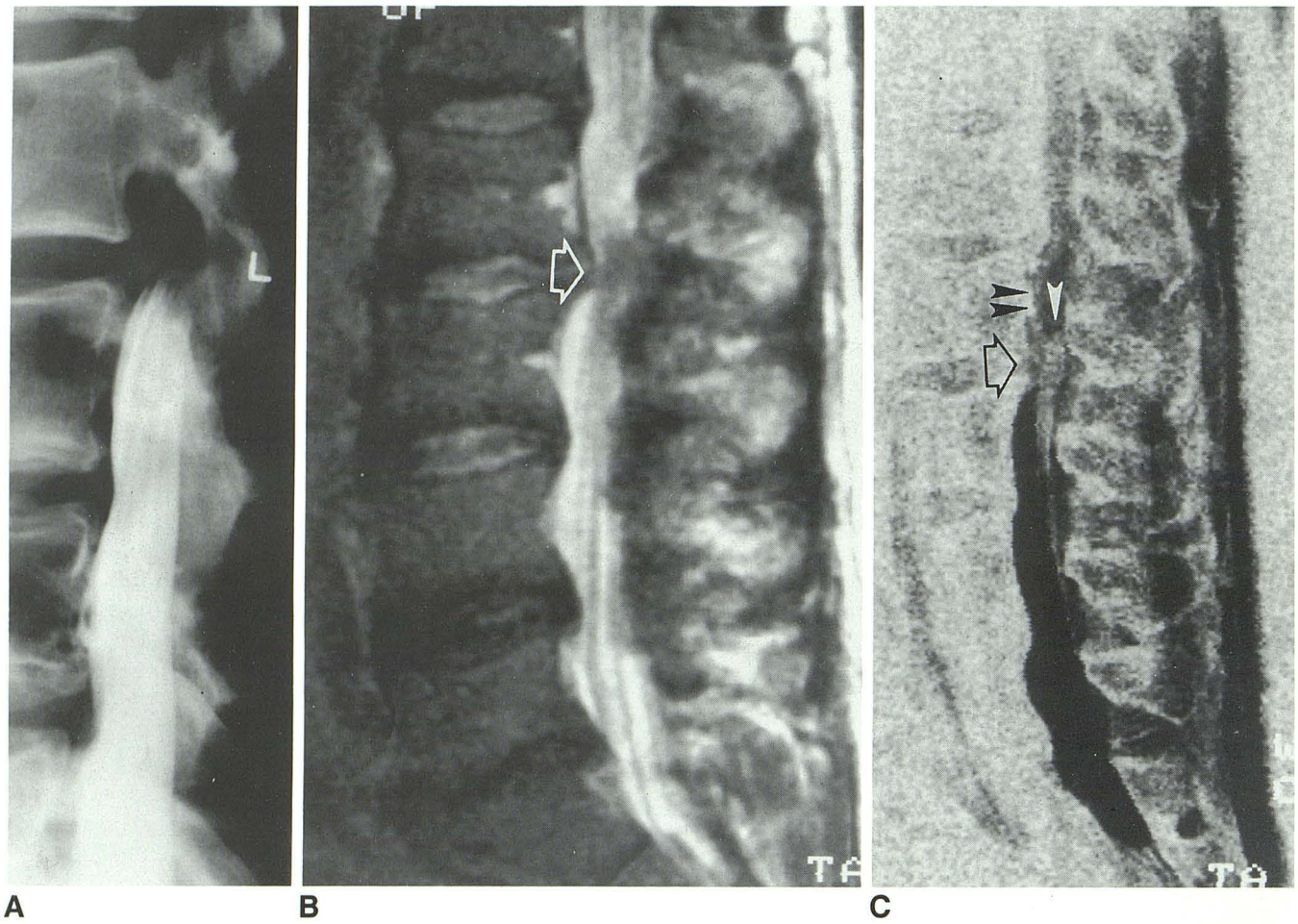

Fig. 7. Type 1 pattern variant. Subtotal block at L2–L3 level secondary to a herniated disk (*open arrow*).

A, Myelogram shows total block of contrast column at L2–L3. In steeper Trendelenburg position, contrast material progressed beyond spinal canal compromise (SCC).

B, T2W spin-echo image shows herniated disk. CSF intensity above and below level of SCC is similar.

C, Slow-flow image shows entire CSF column distal to level of SCC in black. Above the SCC, the CSF compartment anterior to the cauda equina/conus is white (*double black arrowheads*). Posteriorly, it images in black (*single white arrowhead).*

Fig. 8. Type 1 pattern variant. Metastatic process involving a midthoracic vertebra with collapse and ensuing high-grade canal compromise.

A, T2W spin-echo image. Note: thoracic cord leaves image plane distally.

B, Corresponding slow-flow image. CSF distal to lesion is black, cord is white. Anterior CSF compartment above lesion is white, posteriorly it is black.

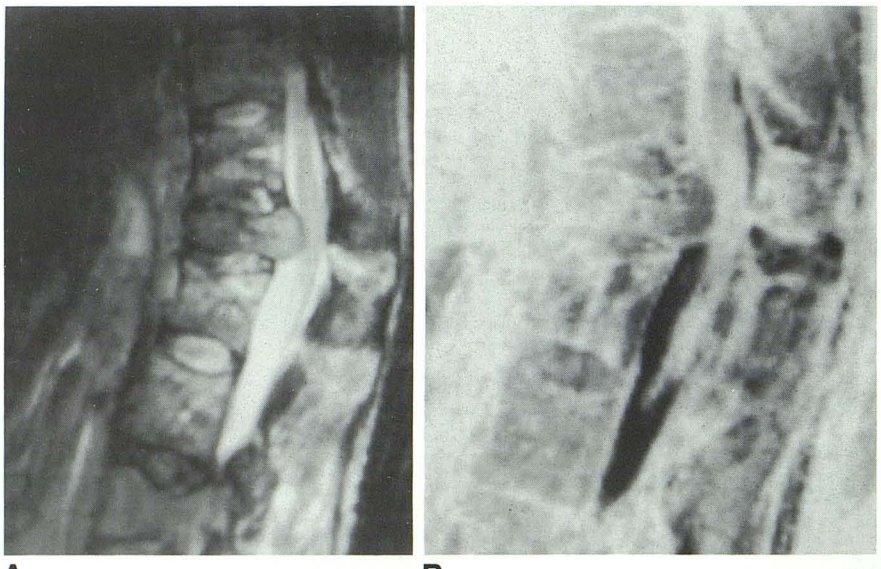

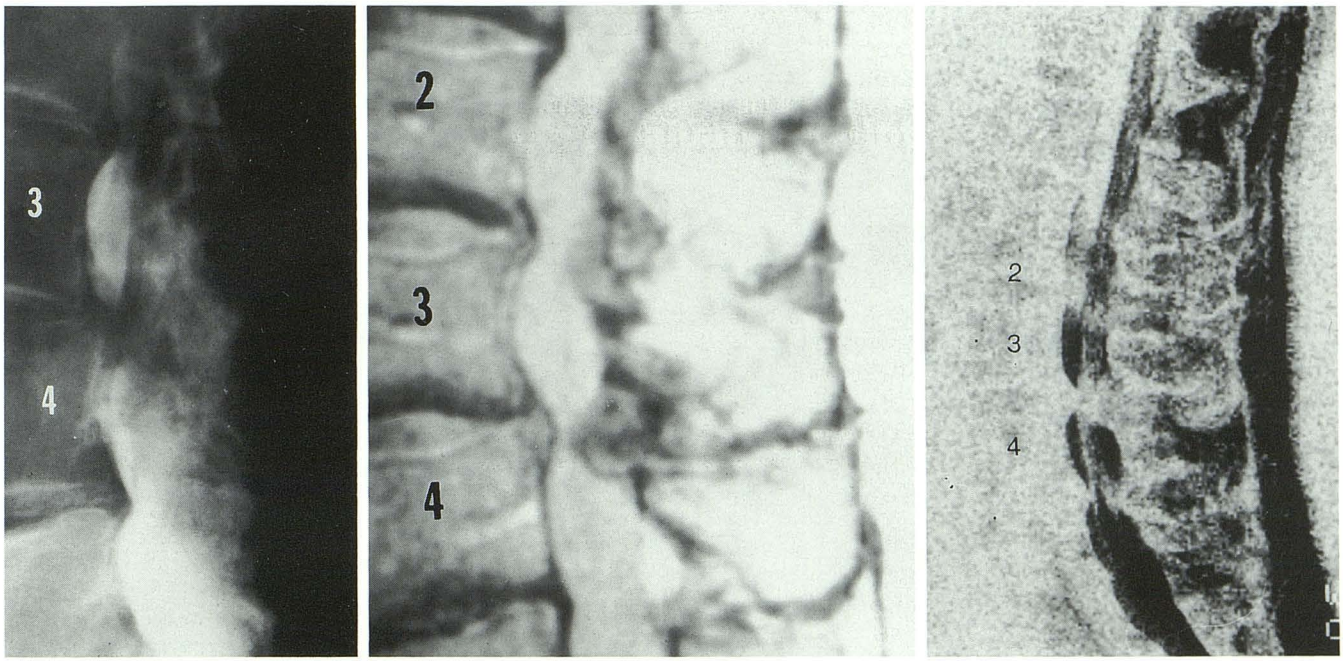

Fig. 9. Type 2 pattern. Degenerative lumbar stenosis, multilevel.

A, Estimated degrees of stenosis by myelography: L2–L3 = 60%+ stenosis; L3–L4 = 90% stenosis; L4–L5 = 20% stenosis.

B, Corresponding proton density image.

C, Corresponding slow-flow image. White CSF column reaches L2–L3 level and becomes black distal to this site. Additional levels of stenosis at L3–L4 and L4–L5 further attenuate CSF velocity, making entire distal CSF space black.

and lumbar region and were either total or subtotal (95%–100%).

A full column of CSF becomes black above and below the site of canal compromise (SCC). Proximal to the SCC, this column measures the height of 1–2 vertebra, sometimes more. Below the SCC, the black CSF column may extend much further (Figs. 5 and 6). Here, the length of the black CSF column depends on the proximity of the SCC to the distal end of the thecal sac. As the SCC approaches the lower end of the canal, the inferior column of black CSF tends to become longer (Fig. 7). With a more proximal SCC, the CSF column immediately below the SCC is black. This segment measures 3–6 cm and is followed by a segment with grayish CSF. More distally, the bright CSF signal is reestablished.

A variant of this pattern was observed in seven areas (cervical and thoracic) where the degree of stenosis was 90%–95%. Myelograms were available for two areas. CSF is again black, both proximal and distal to the SCC. However, black CSF is seen only anterior or posterior to the cord. The opposing CSF column showed variable signals (Figs. 7 and 8).

2. Intermediate Grade Stenosis (50%–89%) (type 2 pattern; Fig. 4; Table 4). There were 13 stenotic sites in this category, six with myelographic evaluation. This pattern showed CSF above the SCC to be white, becoming black below the stenotic site. This was observed in three areas of lumbar stenosis (Fig. 9). A pattern variant was seen in six areas of stenosis, all cervical or thoracic. It showed the signal reversal distal to the block limited to the anterior or posterior CSF compartment; one CSF compartment became black while the opposing CSF space remained white (Fig. 10). Four areas showed normal flow.

3. Low-Grade Stenosis (10%–49%) (type 3 pattern; Fig. 4; Table 4. Twenty-six stenosed areas, seven with myelographic correlation, were in this group. Many patients (n = 15) had normal CSF signals. Focal CSF attenuation was seen in 11 areas of stenosis. This was evidenced by focal, spotty CSF blackening close to the stenosing lesion (Fig. 11).

Discussion

Slow Flow Sequence

As this sequence is based on the loss of steady state caused by the dephasing of moving spins,

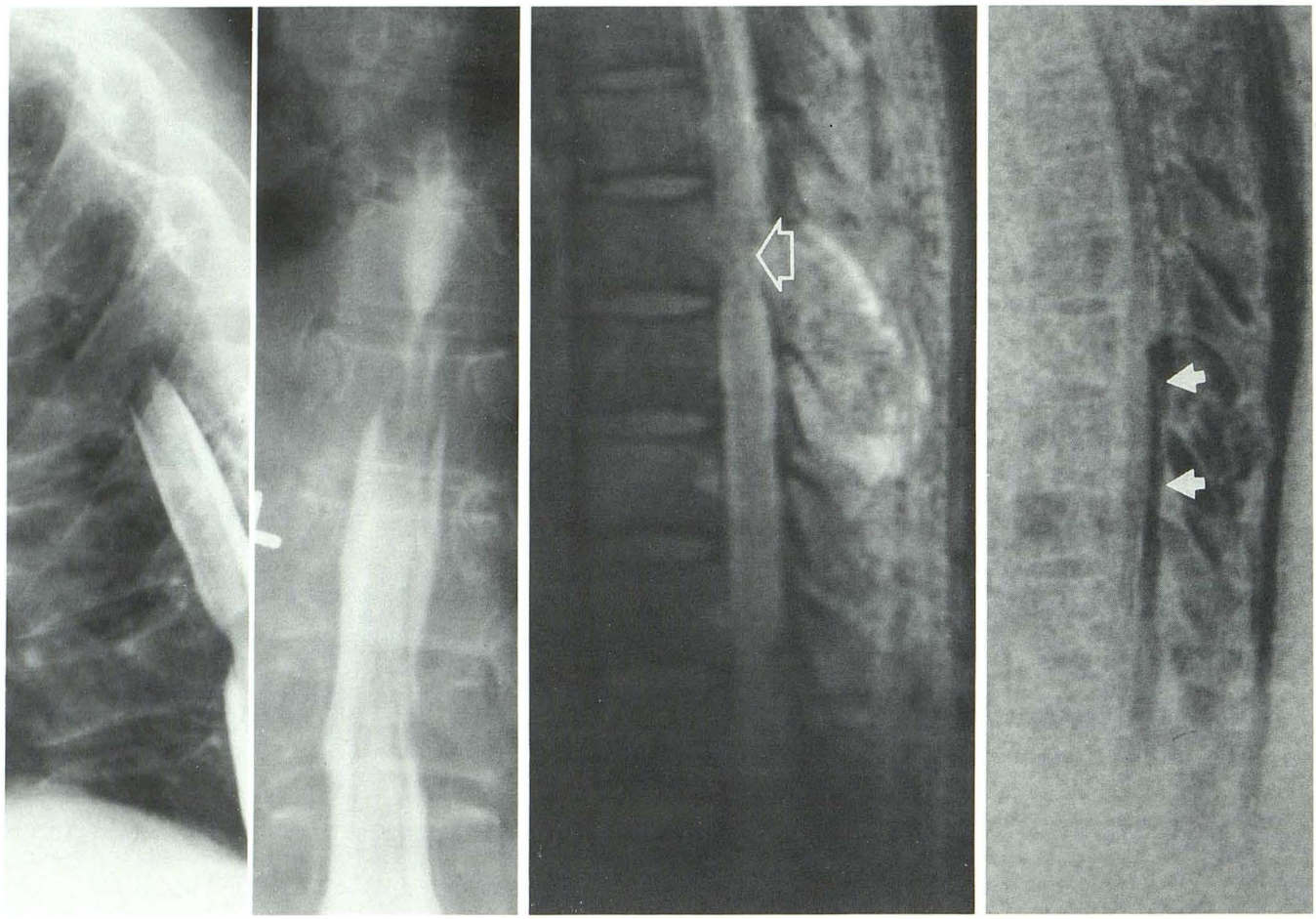

Fig. 10. Type 2 pattern variant. Breast metastases to spinal column. Approximately at T9, there is evidence of spinal canal compromise (SCC) due to metastatic process in one of the spinous processes.

A, Myelogram suggests high-grade stenosis. Contrast is temporarily held up, but advances distally upon further downward tilt.

B, T2W spin-echo image suggest less advanced stenosis (*open arrow*).

C, Slow-flow image shows CSF above SCC in white. Below the SCC, CSF in the anterior compartment is white, but is black posteriorly (*white arrows*), just distal to level of SCC.

the "flow void" effect used here is directly related to flow rather than to the phase dispersion across each voxel produced by a velocity distribution (24–26). It results in a sequence that is much more sensitive to flow than a regular spin-echo sequence. This is true even when the spin-echo sequence is sensitized with additional gradient pulses (27), where flow void effects only results from inhomogenous intravoxel velocities. On the other hand, in the presence of intravoxel velocity dispersion, the effect is added to the flow void and does not result in an artifact, as is common with MR angiography techniques.

A possible drawback of the method is its anisotropic sensitivity. The highest sensitivity of the method is clearly in the direction of the readout gradient. This may be a problem for very slow flow structures if flow is not in the direction of this gradient. Of course, for CSF imaging of the spinal canal, the readout gradient can be oriented along the spinal axis for maximum flow sensitivity. Another limitation is given by the relatively low signal/noise ratio of SSFP sequences. This low signal/noise ratio is increased here by using a 3-D mode, but it may remain too low in structures with short T2s, as found outside the central nervous system. This sequence is quite susceptible to patient motion. Thus, the images may appear noisy. SFMR scans are regarded as functional images and are used solely for the evaluation of flow.

The main advantage of the proposed method, beside its very high sensitivity to slow flow, is its speed. In this study, 16 truly continguous images

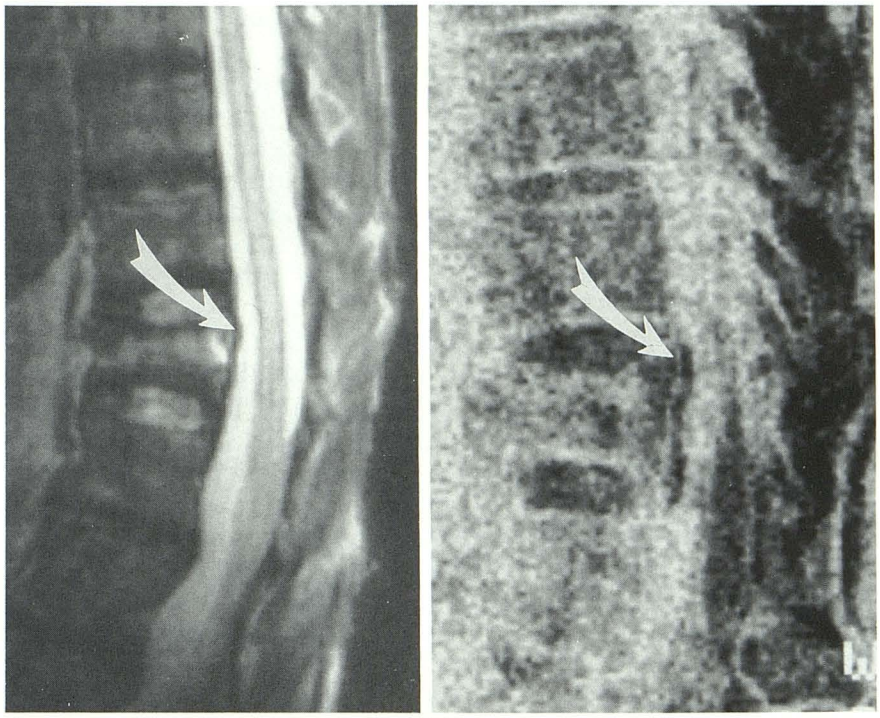

Fig. 11. Type 3 pattern. Compression fracture of T12 with minimal impingement of anterior canal.

A, T2W spin-echo image barely shows minimal identation (*arrow*) at level of the compressed vertebral body.

B, Corresponding slow-flow image shows definite focal blackening of CSF, distal to indentation (*arrow*).

(1-mm spatial resolution, 1.25-mm thickness) were acquired in about 1 minute. No extra hardware is required. Commercial unshielded gradient coils (10 mT/m) were used. The method can thus be applied on a routine basis without adding significant amount of scanning time. Reconstruction of the 2-D images is straightforward, as is display of the contrast reversed images. No substraction is needed. If one wishes to visualize 3-D views, the 2-D images have to be transferred to an off-line running program. A ray-tracer algorithm using minimum intensity projections then could allow projections to be displayed with any angle.

Normal CSF Flow Pattern

The oscillatory motion of CSF in the spinal canal has been studied by various means (1–8, 11, 15). Literature reports put the CSF velocity range for the cervical spine in the range of 3–100 mm/sec (1, 3, 6, 13, 18). The velocity decreases as one descends the spinal axis. In the lumbar area it is found in the range of 0–28 mm/sec (13, 18).

The published CSF velocity data imply that oscillatory motion in the spinal canal is usually above the gray-scale window for the discussed SFMR sequence. Thus, most CSF will be portrayed in white. As the water hammer effect of the pulsating CSF column dissipates in the distal canal, CSF will enter a velocity range of 0–5 mm/sec. The tail end of the CSF column will image in progressing shades of gray. The sacral sac usually holds stagnant CSF and will show in black (Fig. 3).

Canal Compromise

For spinal canal compromise and the associated flow attenuation or arrest, a variable scale of MR signal reduction is anticipated. Of all the observed patterns, the full column CSF stasis above and below the site of stenosis (type 1 pattern) (Figs. 4A, 5, and 6) was the most sensitive and specific. On myelography and standard MR images, it always characterized subtotal or total block. Our observations are consistent with the direct flow measurements by Lane and Kricheff (13) and DuBoulay (1). At some distance, distal to the high-grade stenosis or block, one can expect resumption of CSF flow, due to epidural and cord pulsation. The closer the block approaches the lower end of the canal, the more likely CSF flow will become sufficiently attenuated to become nearly stagnant. Thus, the distal low velocity tail will grow larger the closer the level of blockage approaches the caudal end (Fig. 7). Also, because of the natural CSF flow attenuation in the very distal portion of the lumbar

canal, additional flow reduction by pathologic conditions at or below L5 may not register as a MR flow change. Thus, flow imaging in the distal thecal sac is expected to be less sensitive.

A type 1 pattern variant, showing black CSF above and below the SCC, but also white CSF in the anterior or posterior gutter (Fig. 4B), was only seen in anatomic areas where there was cord, conus, or proximal cauda equina. These structures compartmentalize the CSF space (Fig. 8). The degree of stenosis in these cases was in the range of 90%–95%. It is possible that partial canal patency allowed a jet-like CSF propulsion anterior or posterior to the cord while the opposing CSF compartment remained sufficiently blocked. For unknown reasons, anterior or posterior blocks did not consistently place the attenuated CSF column (black CSF) anteriorly or posteriorly.

Type 2 pattern and its variant (Figs. 4C and 4D) were observed in intermediate stenoses (50%–89%). It was considered typical for this range of canal compromise. However, the pattern is much less sensitive than the type 1 pattern. Four cases did not show any flow changes. It is assumed that lesser stenosis allows the full impact of the proximal CSF water hammer to hit the stenotic level. Consequently, bright (higher velocity) CSF is shown down to the level of stenosis. CSF distal to the SCC becomes sufficiently attenuated to produce black CSF (Fig. 9). The type 2 pattern variant (Fig. 10) showed the distal CSF column with different velocity levels anterior and posterior to the cord. This suggests that canal stenosis can cause different flow velocities in the various CSF compartments.

The flow changes seen with low-grade stenosis (type 3 pattern) (Figs. 4E and 11) merely reflect local flow turbulence and eddies. They are of little diagnostic value for predicting degree of stenosis.

In 1966, du Boulay (1) was able to demonstrate with pneumencephalography and oil-contrast myelography systole-synchronous pulsatile CSF motion. With complete obstruction, all pulsation distal to the SCC ceased, but pulsation persisted on the cranial side. Lane and Kricheff (13) studied CSF motion at myelography by videodensitometric means. At SCCs, the pulsations amplitudes diminished. With canal blockage, there was much lower pulsation above and below, in the range of 0–2 mm/sec. The flow measurements in these early works were obviously limited. However, the findings are entirely consistent with the observations in flow patterns type 1 and 2.

Earlier works in the MR literature (4, 5, 16, 17) recognized flow-void effects in the spinal CSF spaces and observed them at sites of canal stenosis. This is the result of spin motion and reflects higher CSF velocities. Nonpulsating CSF was shown to exhibit a higher signal than does pulsatile CSF. Rubin et al and Enzmann et al (16, 17, 19) in a small sample and Quint (20) in a larger series exploited the absence of CSF pulsation artifacts on T2W spin-echo images for the detection of significant block. Because of the gray-scale reversal on our SFMR sequence, its bright signals can be equated with signal voids on traditional T2W images.

The classical flow-void phenomenon at the aqueduct reflects a CSF pulse velocity of 40–60 mm/sec (4). Rubin et al (19), in phantom experiments, observed flow artifacts with CSF pulse velocities as low as 3 mm/sec. Yet, flow effects were much more obvious at velocity ranges of 10–30 mm/sec. Thus, the flow-void equivalent of our SFMR sequence occurs at lower threshold levels (0.5–5 mm/sec) than those observed on traditional, nongated spin-echo sequences.

MR phase imaging (3, 6, 11) can provide direct means for mapping and quantitation of pulsatile flow. This method uses cardiac gating and samples data at certain points within the cardiac cycle. It is sensitive to velocities as slow as 5 mm/sec. Phase contrast cine (18, 21) adds another dimension to the depiction of CSF flow. The method has been used for visualization of CSF flow compromise in the spinal canal. While this imaging modus is sufficiently rapid, it requires cardiac gating and postprocessing steps for completion. In contrast, SFMR does not require cardiac gating, samples many cardiac cycles, and produces time-average images. Cardiac-gated studies of CSF flow have not been shown superior to nongated studies for clinical diagnosis. Still, for some dynamic and physiologic studies, cardiac gating can be important (8).

Patz et al (7) and Jolesz et al (8) stress that state-free precession is particularly sensitive to slow flow. They found a flow sensitivity on the order of 1 mm/sec along the direction of the read gradient. The method has proven itself in the detection of CSF flow/motion patterns in the clinical diagnosis of forms of hydrocephalus and helped confirm or exclude the presence of ventricular obstruction.

At sites of stenosis, some authors have observed increased velocities (28, 29). This was not seen in our series. Of course, this SFMR sequence

may be blinded to this effect since an increase in velocity would not change CSF brightness that has already peaked at 5 mm/sec.

In this report, 34% of the stenotic sites were also appraised myelographically. The myelographic findings were used mainly to verify the degree of stenosis, as suggested by the standard MR sequences. Since the number of myelographic correlations for the various groups and subgroups were too small, no attempt was made here to compare the accuracy of the two methods. Hypothetically, SFMR may portray canal blockage more accurately than myelography as it provides a direct measurement of CSF flow. Although myelography is commonly accepted as the gold standard, technical factors, such as degree of CSF opacification, positioning, and quality of filming, may severely compromise the accuracy of the method.

In conclusion, high-grade spinal stenosis or block can be reliably diagnosed with SFMR. In situations where patient management depends on a definitive diagnosis of high-grade SSC, SFMR can add important information to the standard MR sequences and promises to make myelography even further expendable.

References

1. Du Boulay GH. Pulsatile movements in the CSF pathways. *Br J Radiol* 1966;39:255–262
2. Bradley WG, Kortman KE, Burgoyne B. Flowing cerebrospinal fluid in normal and hydrocephalic states: appearance on MR images. *Radiology* 1985;159:611–616
3. Edelman RR, Wedeen VJ, Davis KR, et al. Multiphasic MR imaging: a new method for direct imaging of pulsatile CSF flow. *Radiology* 1986;161:779–783
4. Sherman JL, Citrin CM. Magnetic resonance demonstration of normal CSF flow. *AJNR* 1986;7:3–6
5. Sherman JL, Citrin CM, Bozen RJ, Gangarosa RE. MR demonstration of altered cerebrospinal fluid flow by obstructive lesions. *AJNR* 1986; 7:571–579
6. Ridgeway JP, Turnbull LW, Smith MA. Demonstration of pulsatile cerebropsinal fluid flow using magnetic resonance phase imaging. *Br J Radiol* 1987;60:423–427
7. Patz S, Hawkes RC. The application of steady-state free precession in the study of very slow fluid flow. *Magn Reson Med* 1986;3: 140–145
8. Jolesz FA, Patz S, Hawkes RC, Lopez I. Fast imaging of CSF flow/ motion patterns using steady-state free precession (SSFP). *Invest Radiol* 1987;22:761–771
9. Atlas SW, Mark AS, Fram EK. Aqueductal stenosis: evaluation with gradient-echo rapid MR imaging. *Radiology* 1988;169:449–453
10. Maschalchi M, Ciraolo L, Tanfani G, et al. Cardiac-gated phase MR imaging of aqueductal CSF flow. *J Comput Assist Tomogr* 1988;12: 923–926
11. Njemanze PC, Beck OJ. MR gated intracranial CSF dynamics: evaluation of CSF pulsatile flow. *AJNR* 1989;10:77–80
12. Mark AS, Feinberg DA, Brandt-Zawadzki MN. Changes in size and magnetic resonance signal intensity of the cerebral CSF spaces during the cardiac cycle as studied by gated, high-resolution magnetic resonance imaging. *Invest Radiol* 1987;22:290–297
13. Lane B, Kricheff II. Cerebrospinal fluid pulsation at myelography: a videodensitometry study. *Radiology* 1974;110:579–587
14. Sherman JL, Citrin CM, Gangarosa RE, Bowen BJ. The MR appearance of CSF pulsation in the spinal canal. *AJNR* 1986;7:879–884
15. Sherman JL, Barkovich AJ, Citrin CM. The MR appearance of syringomyelia: new observations. *AJNR* 1986;7:985–995
16. Enzmann DR, Rubin JR, DeLaPaz R, Wright A. Cerebrospinal fluid pulsation: benefits and pitfalls in MR imaging. *Radiology* 1986;161: 773–778
17. Rubin JB, Enzmann DR. Imaging of spinal CSF pulsati on by 2 DFT MR: significance during clinical imaging. *AJR* 1987;148:973–982
18. Quencer RM, Donovan Post MJ, Hinks RS. Cine MR in the evaluation of normal and abnormal CSF flow: intracranial and intraspinal studies. *Neuroradiology* 1990;32:371–391
19. Rubin JB, Writh A, Enzman DR. Lumbar spine: motion compensation for cerebrospinal fluid on MR imaging. *Radiology* 1988;166: 225–235
20. Quint DJ, Patel SC, Sanders WP, Herarshen DO, Boulas RS. Importance of absence of CSF pulsation artifacts in the MR detection of significant myelographic block at 1.5 T. *AJNR* 1989;10:1089–1095
21. Levy LM, Di Chiro G. MR phase imaging and cerebrospinal fluid flow in the head and spine. *Neuroradiology* 1990;32:399–406
22. LeBihan D, Schellinger D, Rajan SS, Deveikis JP, Carvlin M, Patronas NJ. Slow flow angiography (abstr). *Magn Reson Imaging* 1990;8:353
23. Hawks RC, Patz S. Rapid fourier imaging using steady-state free precession. *J Magn Reson* 1987;4:9–23
24. Gyngell ML. The application of steady-state free precession in rapid 2DFT NMRI: FAST and CE-Fast sequences. *Magn Reson Imaging* 1988;6:415–419
25. Bradley WE, Waluch V. Blood flow: magnetic resonance imaging. *AJR* 1984;143:1157–1166
26. Bryant DG, Payne JA, Firmin DN, Longmore DB. Measurement of flow with NMR imaging using a gradient pulse and phase difference technique. *J Comput Assit Tomogr* 1984;8:588–593
27. Von Shulthess GK, Higgins CB. Blood flow imaging with MR: spin-phase phenomena. *Radiology* 1985;157:687–695
28. Donovan-Post MJ, Hinks RS, Quencer RM, Green BA. *Cine-MR quantification of spinal CSF flow in the healthy adult.* Annual Scientific Assembly ASNR, 1990, Los Angeles, CA. Program Book:112
29. Itabashi T, Arai S, Kitahura H, Watanabe T, Asahina K, Susuki H. *Quantitative analysis of cervical cerebrospinal fluid pulsation.* Paper presented at the 74th Annual Meeting of the RSNA (Paper #569), November 30, 1988, Chicago, IL